Spin dynamics of itinerant holes in HTSC cuprates: the singlet-correlated band model and its applications

2007 J. Phys.: Condens. Matter 19 116209

(http://iopscience.iop.org/0953-8984/19/11/116209)

IOP PUBLISHING JOURNAL OF PHYSICS: CONDENSED MATTER

J. Phys.: Condens. Matter **19** (2007) 116209 (18pp) doi:10.1088/0953-8984/19/11/116209

Spin dynamics of itinerant holes in HTSC cuprates: the singlet-correlated band model and its applications

T Mayer[1], M Eremin[2], I Eremin[3,4] and P F Meier[1]

[1] Physics Institute, University of Zurich, CH-8055 Zurich, Switzerland
[2] Kazan State University, Kazan 420008, Russia
[3] Max-Planck Institut fur Physik Komplexer Systeme, D-01187 Dresden, Germany
[4] Technische Universitaet Braunschweig, D-38106 Braunschweig, Germany

E-mail: mayer@physik.unizh.ch

Received 4 October 2006, in final form 25 January 2007
Published 5 March 2007
Online at stacks.iop.org/JPhysCM/19/116209

Abstract

So far calculations of the spin susceptibility in the superconducting state of cuprates have been performed in the framework of weak-coupling approximations. However, it is known that cuprates belong to Mott–Hubbard doped materials where electron correlations are important. In this paper an analytical expression for the spin susceptibility in the superconducting state of cuprates is derived within the singlet-correlated band model, which takes into account strong correlations. The expression of the spin susceptibility is evaluated using values for the hopping parameters adapted to measurements of the Fermi surface of the materials $YBa_2Cu_3O_7$ and $Bi_2Sr_2CaCu_2O_8$. We show that the available experimental data which are directly related to the spin susceptibility can be explained consistently within one set of model parameters for each material. These experiments include the magnetic resonance peak observed by inelastic neutron scattering and the temperature dependence of nuclear magnetic resonance properties like the spin shift and the spin–spin and spin–lattice relaxation rates in the superconducting state.

(Some figures in this article are in colour only in the electronic version)

1. Introduction

Derivations of theoretical expressions for the dynamical spin susceptibility of layered cuprates have been in the focus of many investigations, since several experimental quantities are directly related to the spin susceptibility. A large number of data sets of the temperature dependence of various nuclear magnetic resonance (NMR) quantities exist. The Knight shift and the spin–spin and the spin–lattice relaxation rates probe the low-energy limit of the spin susceptibility. Inelastic neutron scattering (INS) measurements in contrast reveal the behaviour of the susceptibility at higher energies. The most complete set of experimental data has been obtained for the YBaCuO compounds.

The theoretical approaches to the spin susceptibility can be divided into two categories, the weak- and strong-coupling models. The former deal with a single-band Hubbard model with the effective Coulomb interaction U_e taken to be of the order of the bandwidth in cuprates. Based on this assumption, the dynamical spin susceptibility can be calculated within a standard random phase approximation (RPA) approach. Extensive studies of NMR and INS data have been carried out within the framework of this model by several groups [1–6]. Initially, the features observed by INS were addressed by Onufrieva *et al* [7, 8] and later by Brinckmann and Lee [9]. However, in both cases the expression for the spin susceptibility was reduced to the conventional RPA-like form which is a crude approximation due to the composite nature of the quasiparticles (no double occupancy constraint).

Recently, a number of studies have been devoted to analysing the spin susceptibility within the strong-coupling t–J model, for which standard many-body perturbative methods do not work. For example the dynamical spin susceptibility was analysed within the slave–boson approximation [10], the Mori–Zwanzig memory function formalism [11] and with the Hubbard X-operators technique [12, 13]. It has been found that, to a large extent, both weak- and strong-coupling calculations give formally very similar results for the spin susceptibility. The respective parameter values, however, differ drastically. Until now, there has also been no complete understanding whether both INS and NMR data can be explained consistently within one model and using the same parameter values of the given theory.

In the present work we analyse these questions in detail. Starting from the singlet-correlated band model, we use a well established decoupling procedure of the equations of motion and approximate higher-order correlation functions so as to obtain an analytical expression for the dynamical spin susceptibility which takes into account strong correlations. In the normal state it coincides with the expression obtained already by Hubbard and Jain [14] who extended their original model to account for strong correlation effects. Their result differs from the conventional Pauli–Lindhard form. Later, Zavidonov and Brinkmann [12] incorporated an additional functional correction for the lower Hubbard sub-band (LHB) model, which also accounts for local spin fluctuation effects. Both of these corrections cannot be included exactly in the RPA approach.

In the present paper we extend the previous analysis and present an analytical expression for the dynamical spin susceptibility in the upper Hubbard sub-band (UHB) in the superconducting state. We perform an extended numerical evaluation of this analytical expression and find that most of the available experimental data which are directly related to the spin susceptibility can be explained consistently within one set of model parameters. These experiments include the magnetic resonance peak observed by INS and the temperature dependence of the NMR spin shift and the spin–spin and the spin–lattice relaxation rates, measured in the superconducting state. Note that in our analysis we restrict ourselves to optimally doped high-temperature superconductors, since the pseudogap phenomenon cannot be explained within our model. Furthermore, in our analysis we take advantage of other available experiments, like the Fermi surface topology that is determined by high-resolution angle-resolved photoemission for various cuprate superconductors. Assuming a $d_{x^2-y^2}$-wave pairing symmetry, we propose an optimal set of parameters for the $YBa_2Cu_3O_7$ and $Bi_2Sr_2CaCu_2O_8$ compounds.

This paper is organized as follows. In section 2 we introduce the model system and present the analytical expression for the spin susceptibility in the superconducting state of cuprates. In sections 3 and 4 we study the spin susceptibility in the singlet-correlated band model by analysing experiments in the superconducting state of the materials $YBa_2Cu_3O_7$ and $Bi_2Sr_2CaCu_2O_8$. A summary and conclusions are given in section 5.

2. Dynamical spin susceptibility in the singlet-correlated band model

The starting point for our calculation is the model Hamiltonian [13, 15]

$$H = \sum_{i,j,\sigma} t_{ij} \psi_i^{pd,\sigma} \psi_j^{\sigma,pd} + \sum_{i>j} J_{ij} \left[(\mathbf{S}_i \mathbf{S}_j) - \frac{n_i n_j}{4} \right] + \sum_{i>j} V_{ij} \delta_i \delta_j, \tag{1}$$

where $\psi_i^{pd,\sigma}$ ($\psi_i^{\sigma,pd}$) are composite copper–oxygen creation (annihilation) operators of the copper–oxygen singlet [16] states in the CuO_2-plane. Furthermore, J_{ij} is the superexchange parameter of the copper spins (this coupling originates from the virtual hopping from the LHB to the UHB via the oxygen state). The number of doped holes is described by $\delta_i = \psi_i^{pd,pd}$ and V_{ij} is an effective density–density interaction parameter. This parameter allows us to account for the screened Coulomb repulsion and phonon (or plasmon) mediated interactions, and it also determines the behaviour of the *charge* susceptibility which was calculated in the normal state in [13]. However, it can be neglected for the *spin* susceptibility because the spin operator commutates with this density–density operator.

We would also like to mention the key difference between the widely known t–J model and the singlet-correlated band model. The conductivity band in the t–J model is constructed on the basis of the $d_{x^2-y^2}$ copper state and the Cu^{3+}-states are included via the superexchange parameter J. In other words the conductivity band is the lower Hubbard sub-band, which is assumed to be completely filled in the parent compounds of high-temperature superconductors. In the singlet-correlated band model the carriers move over the oxygen sites, which is based on experimental evidence [17]. The spins of the oxygens are strongly correlated (singlets) with the copper spins [16, 18], forming a band mainly on the basis of the so-called Zhang–Rice singlets. This singlet-correlated band does not exist in the undoped parent compounds, because of lack of additional doped oxygen holes in the insulating phase. Furthermore, this band is analogous to an upper Hubbard sub-band, with the exception that the energy difference between this singlet-correlated band and the lower Hubbard sub-band is only 1 eV (the copper–oxygen coupling energy), instead of the 6–8 eV in the original Hubbard theory. For a more detailed discussion of the Hubbard and singlet-correlated band models and their band structures see [19] (in particular figures 7–9 therein). We will derive in this section an expression for the spin susceptibility in this upper Hubbard sub-band model which is different from the t–J model.

The susceptibility is calculated from the general expression

$$\chi^{+-}(\mathbf{q}, \omega) = -2\pi \mathrm{i} \left\langle\!\left\langle S_{\mathbf{q}}^{+} \,\middle|\, S_{-\mathbf{q}}^{-} \right\rangle\!\right\rangle, \tag{2}$$

where the spin density operator $S_{\mathbf{q}}^{+}$ for the singlet-correlated band is written as

$$S_{\mathbf{q}}^{+} = \sum_i \psi_i^{\uparrow,\downarrow} \mathrm{e}^{-\mathrm{i}\mathbf{q}\mathbf{R}_i} \simeq \sum_{\mathbf{k}} \psi_{\mathbf{k}+\mathbf{q}}^{\uparrow,pd} \psi_{\mathbf{k}}^{pd,\downarrow}. \tag{3}$$

Here we may drop all the quasiparticle creation (annihilation) operators $\psi_i^{0,\sigma}$ ($\psi_i^{\sigma,0}$) corresponding to the LHB, because this band is assumed to be completely filled.

The expression for the susceptibility is derived by the following procedure. First, we write down a complete set of equations of motion using the composite copper–oxygen creation (annihilation) operators $\psi_i^{pd,\sigma}$ ($\psi_i^{\sigma,pd}$) of the copper–oxygen singlet states in the plane. Then, by means of a linear transformation we rearrange these equations via Bogoliubov's quasiparticle operators into new sets of equations, which finally will be solved. An expression for the susceptibility was previously derived [15] by utilizing the method of Heisenberg equations of motion in a small magnetic field. The advantage of the Green's function method is that it allows one to obtain a formula for the susceptibility which contains both the itinerant (or quasi-Fermi-liquid) part and the local spin fluctuation part in one general expression.

The equation of motion for the relevant Green's function in the normal state ($T > T_c$) has been derived before by some of us [13]. It is given by

$$\begin{aligned}\omega\left\langle\!\left\langle -\psi_{\mathbf{k}}^{pd,\downarrow}\psi_{\mathbf{k+q}}^{\uparrow,pd}\,|S_{-\mathbf{q}}^{-}\right\rangle\!\right\rangle &= \frac{\mathrm{i}}{2\pi}\left(\left\langle\psi_{\mathbf{k}}^{pd,\downarrow}\psi_{\mathbf{k}}^{\downarrow,pd}\right\rangle - \left\langle\psi_{\mathbf{k+q}}^{pd,\uparrow}\psi_{\mathbf{k+q}}^{\uparrow,pd}\right\rangle\right)\\ &- \left(\varepsilon_{\mathbf{k}}-\varepsilon_{\mathbf{k+q}}\right)\left\langle\!\left\langle -\psi_{\mathbf{k}}^{pd,\downarrow}\psi_{\mathbf{k+q}}^{\uparrow,pd}\,|S_{-\mathbf{q}}^{-}\right\rangle\!\right\rangle\\ &+ \frac{1}{N}\left\{\left(J_{\mathbf{q}}-t_{\mathbf{k}}\right)\left\langle\psi_{\mathbf{k}}^{pd,\downarrow}\psi_{\mathbf{k}}^{\downarrow,pd}\right\rangle\right.\\ &\left.- \left(J_{\mathbf{q}}-t_{\mathbf{k+q}}\right)\left\langle\psi_{\mathbf{k+q}}^{pd,\uparrow}\psi_{\mathbf{k+q}}^{\uparrow,pd}\right\rangle\right\}\left\langle\!\left\langle S_{\mathbf{q}}^{+}\,|S_{-\mathbf{q}}^{-}\right\rangle\!\right\rangle\\ &+ \frac{P}{N}\sum_{\mathbf{k}'}\left(t_{\mathbf{k}'+\mathbf{q}}-t_{\mathbf{k}'}\right)\left\langle\!\left\langle\psi_{\mathbf{k}'}^{pd,\downarrow}\psi_{\mathbf{k}'+\mathbf{q}}^{\uparrow,pd}\,|S_{-\mathbf{q}}^{-}\right\rangle\!\right\rangle, \end{aligned}\tag{4}$$

where the factor $P = (1+\delta)/2$ is a doping-dependent constant which arises due to the narrowing of the band in the so-called Hubbard-I approximation.

In addition to (4) it has been shown [13] that

$$\omega\left\langle\!\left\langle S_{\mathbf{q}}^{+}\,|S_{-\mathbf{q}}^{-}\right\rangle\!\right\rangle = \sum_{\mathbf{k}'}\left(t_{\mathbf{k}'}-t_{\mathbf{k}'+\mathbf{q}}\right)\left\langle\!\left\langle\psi_{\mathbf{k}'}^{pd,\downarrow}\psi_{\mathbf{k}'+\mathbf{q}}^{\uparrow,pd}\,|S_{-\mathbf{q}}^{-}\right\rangle\!\right\rangle.\tag{5}$$

Therefore, if we combine (4) and (5) we get

$$\begin{aligned}\omega\left\langle\!\left\langle -\psi_{\mathbf{k}}^{pd,\downarrow}\psi_{\mathbf{k+q}}^{\uparrow,pd}\,|S_{-\mathbf{q}}^{-}\right\rangle\!\right\rangle &= \frac{\mathrm{i}}{2\pi}\left(\left\langle\psi_{\mathbf{k}}^{pd,\downarrow}\psi_{\mathbf{k}}^{\downarrow,pd}\right\rangle - \left\langle\psi_{\mathbf{k+q}}^{pd,\uparrow}\psi_{\mathbf{k+q}}^{\uparrow,pd}\right\rangle\right)\\ &- \left(\varepsilon_{\mathbf{k}}-\varepsilon_{\mathbf{k+q}}\right)\left\langle\!\left\langle -\psi_{\mathbf{k}}^{pd,\downarrow}\psi_{\mathbf{k+q}}^{\uparrow,pd}\,|S_{-\mathbf{q}}^{-}\right\rangle\!\right\rangle\\ &+ \frac{1}{N}\left\{\left(J_{\mathbf{q}}-t_{\mathbf{k}}\right)\left\langle\psi_{\mathbf{k}}^{pd,\downarrow}\psi_{\mathbf{k}}^{\downarrow,pd}\right\rangle\right.\\ &\left.- \left(J_{\mathbf{q}}-t_{\mathbf{k+q}}\right)\left\langle\psi_{\mathbf{k+q}}^{pd,\uparrow}\psi_{\mathbf{k+q}}^{\uparrow,pd}\right\rangle\right\}\left\langle\!\left\langle S_{\mathbf{q}}^{+}\,|S_{-\mathbf{q}}^{-}\right\rangle\!\right\rangle\\ &- \frac{P}{N}\omega\left\langle\!\left\langle S_{\mathbf{q}}^{+}\,|S_{-\mathbf{q}}^{-}\right\rangle\!\right\rangle. \end{aligned}\tag{6}$$

The equation of motion (6) makes it possible to derive the expression of the dynamical spin susceptibility in the normal state [13].

For the superconducting state we need to perform Bogoliubov's transformation

$$\begin{aligned}\alpha_{\mathbf{k}}^{pd,\downarrow} &= u_{\mathbf{k}}\psi_{\mathbf{k}}^{pd,\downarrow} - v_{\mathbf{k}}\psi_{-\mathbf{k}}^{\uparrow,pd}\\ \alpha_{\mathbf{k}}^{pd,\uparrow} &= u_{\mathbf{k}}\psi_{\mathbf{k}}^{pd,\uparrow} + v_{\mathbf{k}}\psi_{-\mathbf{k}}^{\downarrow,pd}.\end{aligned}\tag{7}$$

Consequently, the spin operator for the superconducting state will be written as

$$\begin{aligned}S_{\mathbf{q}}^{+} = &\sum_{\mathbf{k}}\left(u_{\mathbf{k+q}}u_{\mathbf{k}}\alpha_{\mathbf{k+q}}^{\uparrow,pd}\alpha_{\mathbf{k}}^{pd,\downarrow} + v_{\mathbf{k}}u_{\mathbf{k+q}}\alpha_{\mathbf{k+q}}^{\uparrow,pd}\alpha_{-\mathbf{k}}^{\uparrow,pd}\right)\\ &- \sum_{\mathbf{k}}\left(u_{\mathbf{k}}v_{\mathbf{k+q}}\alpha_{-\mathbf{k}-\mathbf{q}}^{pd,\downarrow}\alpha_{\mathbf{k}}^{pd,\downarrow} + v_{\mathbf{k}}v_{\mathbf{k+q}}\alpha_{-\mathbf{k}-\mathbf{q}}^{pd,\downarrow}\alpha_{-\mathbf{k}}^{\uparrow,pd}\right).\end{aligned}\tag{8}$$

Therefore in the superconducting state we need to construct additional equations for the Green's functions $\langle\langle -\alpha_{\mathbf{k}}^{pd,\downarrow}\alpha_{\mathbf{k+q}}^{\uparrow,pd}|S_{-\mathbf{q}}^{-}\rangle\rangle$, $\langle\langle -\alpha_{-\mathbf{k}}^{\uparrow,pd}\alpha_{\mathbf{k+q}}^{\uparrow,pd}|S_{-\mathbf{q}}^{-}\rangle\rangle$, $\langle\langle \alpha_{\mathbf{k}}^{pd,\downarrow}\alpha_{-\mathbf{k}-\mathbf{q}}^{pd,\downarrow}|S_{-\mathbf{q}}^{-}\rangle\rangle$ and $\langle\langle \alpha_{-\mathbf{k}}^{\uparrow,pd}\alpha_{-\mathbf{k}-\mathbf{q}}^{pd,\downarrow}|S_{-\mathbf{q}}^{-}\rangle\rangle$. Each of them has to be expressed via the $\psi_{\mathbf{k}}^{pd,\sigma}$ operators, for example

$$\begin{aligned}\left\langle\!\left\langle -\alpha_{\mathbf{k}}^{pd,\downarrow}\alpha_{\mathbf{k+q}}^{\uparrow,pd}\,|S_{-\mathbf{q}}^{-}\right\rangle\!\right\rangle &= -u_{\mathbf{k}}u_{\mathbf{k+q}}\left\langle\!\left\langle\psi_{\mathbf{k}}^{pd,\downarrow}\psi_{\mathbf{k+q}}^{\uparrow,pd}\,|S_{-\mathbf{q}}^{-}\right\rangle\!\right\rangle\\ &+ v_{\mathbf{k}}u_{\mathbf{k+q}}\left\langle\!\left\langle\psi_{-\mathbf{k}}^{\uparrow,pd}\psi_{\mathbf{k+q}}^{\uparrow,pd}\,|S_{-\mathbf{q}}^{-}\right\rangle\!\right\rangle\end{aligned}$$

$$- u_{\mathbf{k}} v_{\mathbf{k+q}} \left\langle\!\left\langle \psi^{pd,\downarrow}_{\mathbf{k}} \psi^{pd,\downarrow}_{\mathbf{-k-q}} \,|S^{-}_{\mathbf{-q}}\right\rangle\!\right\rangle$$
$$+ v_{\mathbf{k}} v_{\mathbf{k+q}} \left\langle\!\left\langle \psi^{\uparrow,pd}_{\mathbf{-k}} \psi^{pd,\downarrow}_{\mathbf{-k-q}} \,|S^{-}_{\mathbf{-q}}\right\rangle\!\right\rangle. \tag{9}$$

Doing so we get

$$\begin{aligned}\omega \left\langle\!\left\langle -\psi^{pd,\downarrow}_{\mathbf{k}} \psi^{\uparrow,pd}_{\mathbf{k+q}} \,|S^{-}_{\mathbf{-q}}\right\rangle\!\right\rangle &= \frac{\mathrm{i}}{2\pi}\left(\left\langle \psi^{pd,\downarrow}_{\mathbf{k}} \psi^{\downarrow,pd}_{\mathbf{k}}\right\rangle - \left\langle \psi^{pd,\uparrow}_{\mathbf{k+q}} \psi^{\uparrow,pd}_{\mathbf{k+q}}\right\rangle\right) \\ &+ \left\langle\!\left\langle \left[-\psi^{pd,\downarrow}_{\mathbf{k}} \psi^{\uparrow,pd}_{\mathbf{k+q}}, H\right] \middle| S^{-}_{\mathbf{-q}}\right\rangle\!\right\rangle_{\mathrm{tr}} \\ &+ \frac{1}{N}\left\{\left(J_{\mathbf{q}} - t_{\mathbf{k}}\right)\left\langle \psi^{\downarrow,pd}_{\mathbf{k}} \psi^{pd,\downarrow}_{\mathbf{k}}\right\rangle \right. \\ &- \left.\left(J_{\mathbf{q}} - t_{\mathbf{k+q}}\right)\left\langle \psi^{pd,\uparrow}_{\mathbf{k+q}} \psi^{\uparrow,pd}_{\mathbf{k+q}}\right\rangle\right\} \left\langle\!\left\langle S^{+}_{\mathbf{q}} \,|S^{-}_{\mathbf{-q}}\right\rangle\!\right\rangle \\ &- \frac{P}{N}\omega \left\langle\!\left\langle S^{+}_{\mathbf{q}} \,|S^{-}_{\mathbf{-q}}\right\rangle\!\right\rangle, \end{aligned} \tag{10}$$

and similar expressions can be obtained for $\langle\langle \psi^{\uparrow,pd}_{\mathbf{-k}} \psi^{\uparrow,pd}_{\mathbf{k+q}} | S^{-}_{\mathbf{-q}}\rangle\rangle$, $\langle\langle \psi^{pd,\downarrow}_{\mathbf{k}} \psi^{pd,\downarrow}_{\mathbf{-k-q}} | S^{-}_{\mathbf{-q}}\rangle\rangle$ and $\langle\langle \psi^{\uparrow,pd}_{\mathbf{-k}} \psi^{pd,\downarrow}_{\mathbf{-k-q}} | S^{-}_{\mathbf{-q}}\rangle\rangle$. Equation (10) has the same form as in the normal state ((6)), except that it is now adapted to be applied for the superconducting state. We note that in the conventional Fermi-liquid theory the anticommutator rule is given as $c_{\mathbf{k}\sigma} c^{\dagger}_{\mathbf{k}\sigma} + c^{\dagger}_{\mathbf{k}\sigma} c_{\mathbf{k}\sigma} = 1$. In the strong-coupling limit, however, this rule is modified [18] due to the Coulomb repulsion. For this reason we have abbreviated the terms which are present in the conventional weak-coupling Fermi-liquid approach in the superconducting state by the truncated Green's function $\langle\langle [-\psi^{pd,\downarrow}_{\mathbf{k}} \psi^{\uparrow,pd}_{\mathbf{k+q}}, H] | S^{-}_{\mathbf{-q}}\rangle\rangle_{\mathrm{tr}}$. The other terms on the right-hand side of (10) are due to the spin modulation $S^{+}_{\mathbf{q}}$.

With the help of these equations we are able to construct the equations of motion which are needed to calculate the spin susceptibility in the superconducting state. The first one is given as

$$\begin{aligned}\left(\omega - E_{\mathbf{p}} + E_{\mathbf{k}}\right)\left\langle\!\left\langle \alpha^{pd,\downarrow}_{\mathbf{k}} \alpha^{\uparrow,pd}_{\mathbf{p}} \,|S^{-}_{\mathbf{-q}}\right\rangle\!\right\rangle &= \frac{\mathrm{i}}{2\pi}\left(u_{\mathbf{k}} u_{\mathbf{p}} + v_{\mathbf{k}} v_{\mathbf{p}}\right)\left(n_{\mathbf{p}} - n_{\mathbf{k}}\right) \\ &+ \frac{1}{N}\left(u_{\mathbf{k}} u_{\mathbf{p}} + v_{\mathbf{k}} v_{\mathbf{p}}\right)\left\{\left(J_{\mathbf{q}} - t_{\mathbf{p}}\right) n_{\mathbf{p}} \right. \\ &- \left.\left(J_{\mathbf{q}} - t_{\mathbf{k}}\right) n_{\mathbf{k}}\right\} \left\langle\!\left\langle S^{+}_{\mathbf{q}} \,|S^{-}_{\mathbf{-q}}\right\rangle\!\right\rangle \\ &+ \left(P_{\mathrm{eff}} - 1\right)\left(u_{\mathbf{k}} u_{\mathbf{p}} + v_{\mathbf{k}} v_{\mathbf{p}}\right) \frac{\omega}{N} \left\langle\!\left\langle S^{+}_{\mathbf{q}} \,|S^{-}_{\mathbf{-q}}\right\rangle\!\right\rangle, \end{aligned} \tag{11}$$

and similar expressions occur for $\langle\langle \alpha^{\uparrow,pd}_{\mathbf{-k}} \alpha^{pd,\downarrow}_{\mathbf{-p}} | S^{-}_{\mathbf{-q}}\rangle\rangle$, $\langle\langle \alpha^{\uparrow,pd}_{\mathbf{-k}} \alpha^{\uparrow,pd}_{\mathbf{p}} | S^{-}_{\mathbf{-q}}\rangle\rangle$ and $\langle\langle \alpha^{pd,\downarrow}_{\mathbf{k}} \alpha^{pd,\downarrow}_{\mathbf{-p}} | S^{-}_{\mathbf{-q}}\rangle\rangle$. Here we have introduced P_{eff}, which is determined by $\varepsilon_{\mathbf{k}} = P_{\mathrm{eff}} t_{\mathbf{k}}$. Note that in the case of weak-coupling approximation P_{eff} reduce to 1. Furthermore, $n_{\mathbf{k}} = \langle \alpha^{pd,\uparrow}_{\mathbf{k}} \alpha^{\uparrow,pd}_{\mathbf{k}}\rangle = \langle \alpha^{pd,\downarrow}_{\mathbf{k}} \alpha^{\downarrow,pd}_{\mathbf{k}}\rangle$ are the occupation numbers in the superconducting state. We further make use of the identity

$$\begin{aligned}\left\langle\!\left\langle S^{+}_{\mathbf{q}} \,|S^{-}_{\mathbf{-q}}\right\rangle\!\right\rangle &= -\sum_{\mathbf{k}} u_{\mathbf{k+q}} u_{\mathbf{k}} \left\langle\!\left\langle \alpha^{pd,\downarrow}_{\mathbf{k}} \alpha^{\uparrow,pd}_{\mathbf{k+q}} \,|S^{-}_{\mathbf{-q}}\right\rangle\!\right\rangle \\ &+ \sum_{\mathbf{k}} v_{\mathbf{k+q}} u_{\mathbf{k}} \left\langle\!\left\langle \alpha^{pd,\downarrow}_{\mathbf{k}} \alpha^{pd,\downarrow}_{\mathbf{-k-q}} \,|S^{-}_{\mathbf{-q}}\right\rangle\!\right\rangle \\ &- \sum_{\mathbf{k}} u_{\mathbf{k+q}} v_{\mathbf{k}} \left\langle\!\left\langle \alpha^{\uparrow,pd}_{\mathbf{-k}} \alpha^{\uparrow,pd}_{\mathbf{k+q}} \,|S^{-}_{\mathbf{-q}}\right\rangle\!\right\rangle \\ &+ \sum_{\mathbf{k}} v_{\mathbf{k+q}} v_{\mathbf{k}} \left\langle\!\left\langle \alpha^{\uparrow,pd}_{\mathbf{-k}} \alpha^{pd,\downarrow}_{\mathbf{-k-q}} \,|S^{-}_{\mathbf{-q}}\right\rangle\!\right\rangle. \end{aligned} \tag{12}$$

With help of this relation the susceptibility is calculated as

$$\chi^{+,-}(\mathbf{q},\omega)=\frac{\chi_0^{+,-}(\mathbf{q},\omega)}{1+J_{\mathbf{q}}\chi_0^{+,-}(\mathbf{q},\omega)+\Pi(\mathbf{q},\omega)+Z(\mathbf{q},\omega)}, \tag{13}$$

where the superexchange interaction between the copper spins is $J_{\mathbf{q}}=J_1(\cos q_x+\cos q_y)$, with J_1 being the superexchange interaction parameter between the nearest-neighbour copper spins. By closer examination of (13) it is evident that the spin susceptibility is fundamentally different form the conventional RPA [1–5] and the lower Hubbard sub-band case [12].

The function $\chi_0^{+,-}(\mathbf{q},\omega)$ is a BCS-like susceptibility and $\Pi(\mathbf{q},\omega)$ is a function which results from strong correlation effects and has been determined [15] before. It is given by

$$\begin{aligned}\Pi(\mathbf{q},\omega)=&\frac{P}{N}\sum_{\mathbf{k}}\left(x_{\mathbf{k}}x_{\mathbf{k+q}}+z_{\mathbf{k}}z_{\mathbf{k+q}}\right)\frac{t_{\mathbf{k}}f_{\mathbf{k}}-t_{\mathbf{k+q}}f_{\mathbf{k+q}}}{\omega+\mathrm{i}\Gamma+E_{\mathbf{k}}-E_{\mathbf{k+q}}}\\&+\frac{P}{N}\sum_{\mathbf{k}}\left(y_{\mathbf{k}}y_{\mathbf{k+q}}+z_{\mathbf{k}}z_{\mathbf{k+q}}\right)\frac{t_{\mathbf{k}}\left(1-f_{\mathbf{k}}\right)-t_{\mathbf{k+q}}\left(1-f_{\mathbf{k+q}}\right)}{\omega+\mathrm{i}\Gamma-E_{\mathbf{k}}+E_{\mathbf{k+q}}}\\&+\frac{P}{N}\sum_{\mathbf{k}}\left(x_{\mathbf{k}}y_{\mathbf{k+q}}-z_{\mathbf{k}}z_{\mathbf{k+q}}\right)\frac{t_{\mathbf{k}}f_{\mathbf{k}}-t_{\mathbf{k+q}}\left(1-f_{\mathbf{k+q}}\right)}{\omega+\mathrm{i}\Gamma+E_{\mathbf{k}}+E_{\mathbf{k+q}}}\\&+\frac{P}{N}\sum_{\mathbf{k}}\left(y_{\mathbf{k}}x_{\mathbf{k+q}}-z_{\mathbf{k}}z_{\mathbf{k+q}}\right)\frac{t_{\mathbf{k}}\left(1-f_{\mathbf{k}}\right)-t_{\mathbf{k+q}}f_{\mathbf{k+q}}}{\omega+\mathrm{i}\Gamma-E_{\mathbf{k}}-E_{\mathbf{k+q}}}.\end{aligned} \tag{14}$$

The function $Z(\mathbf{q},\omega)$ has its origin in the fast fluctuation of the localized spins and it is calculated as

$$\begin{aligned}Z(\mathbf{q},\omega)=&\frac{(P_{\mathrm{eff}}-1)}{N}\sum_{\mathbf{k}}\left(x_{\mathbf{k}}x_{\mathbf{k+q}}+z_{\mathbf{k}}z_{\mathbf{k+q}}\right)\frac{\omega+\mathrm{i}\Gamma}{\omega+\mathrm{i}\Gamma+E_{\mathbf{k}}-E_{\mathbf{k+q}}}\\&+\frac{(P_{\mathrm{eff}}-1)}{N}\sum_{\mathbf{k}}\left(y_{\mathbf{k}}y_{\mathbf{k+q}}+z_{\mathbf{k}}z_{\mathbf{k+q}}\right)\frac{\omega+\mathrm{i}\Gamma}{\omega+\mathrm{i}\Gamma-E_{\mathbf{k}}+E_{\mathbf{k+q}}}\\&+\frac{(P_{\mathrm{eff}}-1)}{N}\sum_{\mathbf{k}}\left(x_{\mathbf{k}}y_{\mathbf{k+q}}-z_{\mathbf{k}}z_{\mathbf{k+q}}\right)\frac{\omega+\mathrm{i}\Gamma}{\omega+\mathrm{i}\Gamma+E_{\mathbf{k}}+E_{\mathbf{k+q}}}\\&+\frac{(P_{\mathrm{eff}}-1)}{N}\sum_{\mathbf{k}}\left(y_{\mathbf{k}}x_{\mathbf{k+q}}-z_{\mathbf{k}}z_{\mathbf{k+q}}\right)\frac{\omega+\mathrm{i}\Gamma}{\omega+\mathrm{i}\Gamma-E_{\mathbf{k}}-E_{\mathbf{k+q}}},\end{aligned} \tag{15}$$

where the functions $x_{\mathbf{k}}=u_{\mathbf{k}}^2=\frac{1}{2}(1+\varepsilon_{\mathbf{k}}/E_{\mathbf{k}})$, $y_{\mathbf{k}}=v_{\mathbf{k}}^2=\frac{1}{2}(1-\varepsilon_{\mathbf{k}}/E_{\mathbf{k}})$ and $z_{\mathbf{k}}=u_{\mathbf{k}}v_{\mathbf{k}}=\Delta_{\mathbf{k}}/(2E_{\mathbf{k}})$ are the conventional coherence factors. Furthermore, Γ is an artificially introduced damping constant and $E_{\mathbf{k}}=\sqrt{(\varepsilon_{\mathbf{k}}-\mu)^2+\Delta_{\mathbf{k}}^2}$ is the energy of Bogoliubov's quasiparticles in the superconducting state. The energy dispersion in the tight-binding approximation for a quadratic two-dimensional lattice is given as

$$\begin{aligned}\varepsilon_{\mathbf{k}}=P_{\mathrm{eff}}\big[&2t_1(\cos k_x+\cos k_y)+4t_2(\cos k_x\cos k_y)\\&+2t_3\left(\cos 2k_x+\cos 2k_y\right)+2t_4\left(\cos 2k_x\cos k_y+\cos 2k_y\cos k_x\right)\\&+4t_5\left(\cos 2k_x\cos 2k_y\right)\big],\end{aligned} \tag{16}$$

where the model parameters $t_1, t_2\ldots$ correspond to nearest-neighbour (NN), next-nearest-neighbour (NNN), and further distant hopping, respectively. For simplicity we do not consider hopping between layers. Further we note that at optimal doping the number of doped holes per unit cell in one CuO_2-layer is $\delta\simeq 0.165$. In bilayer compounds therefore we have $\delta=0.33$ with a corresponding factor $P_{\mathrm{eff}}=P=(1+\delta)/2\simeq 0.7$ near optimal doping.

Let us consider the impact of the new functional corrections $\Pi(\mathbf{q},\omega)$ and $Z(\mathbf{q},\omega)$ on the spin susceptibility. In figure 1 we show the real part of the susceptibility along with results for

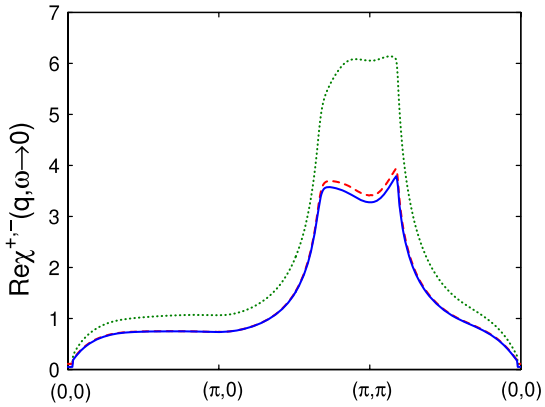

Figure 1. Real part of the spin susceptibility $\chi^{+,-}(\mathbf{q},\omega)$ (solid curve) over the Brillouin zone for $YBa_2Cu_3O_7$ at $T = 0.2T_c$. The results for $Z(\mathbf{q},\omega) = 0$ (dashed curve) and $\Pi(\mathbf{q},\omega) = 0$ (dotted curve) are also shown. The corresponding model parameters are summarized in table 1.

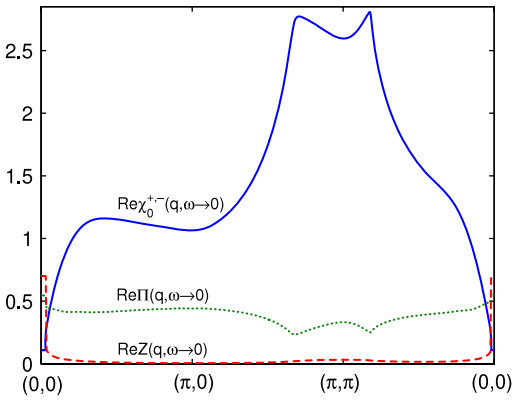

Figure 2. Real part of the BCS susceptibility $\chi_0^{+,-}(\mathbf{q},\omega)$ (solid curve) and the functions $\Pi(\mathbf{q},\omega)$ (dotted curve), $Z(\mathbf{q},\omega)$ (dashed curve) along the Brillouin zone for $YBa_2Cu_3O_7$ at $T = 0.2T_c$. The corresponding model parameters are summarized in table 1.

the cases $Z(\mathbf{q},\omega) = 0$ and $\Pi(\mathbf{q},\omega) = 0$. The immediate consequence of these corrections is that the susceptibility becomes suppressed around (π,π). This can be understood, for example, by the examination of the functional form of $\Pi(\mathbf{q},\omega)$, which in first approximation is $\Pi(\mathbf{q},\omega) \simeq \delta/P - t_{\mathbf{k}}\chi_0^{+,-}(\mathbf{q},\omega)$. This relation can be verified by an inspection of figure 2, where we have plotted the real part of the BCS susceptibility $\chi_0^{+,-}(\mathbf{q},\omega)$ along with the real parts of $\Pi(\mathbf{q},\omega)$ and $Z(\mathbf{q},\omega)$. Therefore the function $\Pi(\mathbf{q},\omega)$ is indeed a significant correction for the spin susceptibility. Another important consequence which can be seen immediately from the figure concerns the $Z(\mathbf{q},\omega)$ function. In the special limit $\mathbf{q} \to 0$, $\omega = 0$, the real part of this function can be approximated as $Z(\mathbf{q} \to 0, \omega = 0) \simeq P = 0.7$ states eV^{-1}. This value is comparable to $\chi_0^{+,-}(\mathbf{q} \to 0, \omega = 0)$ and therefore of importance for the calculation of the Knight shift.

Furthermore, we would like to point out that our model for the spin susceptibility (solid line in figure 1) is in remarkably good agreement with the RPA result [3, 6]. However, in the RPA theory a very large value of the interaction parameter is used: $U_e \simeq 2t_1 \simeq 400$ meV. In our model, which includes strong correlation effects, we need only $J_1 \simeq 0.5t_1 \simeq 100$ meV to arrive at the same absolute values for the spin susceptibility ($\approx$4 states eV^{-1} around (π,π)).

The mechanism that causes the pairing in cuprates is still being debated and the origin of the interactions described by V_{ij} in (1) are unknown. Therefore we introduce the superconducting gap function $\Delta_{\mathbf{k}}$ phenomenologically into our model. Assuming a $d_{x^2-y^2}$ pairing symmetry it is given by

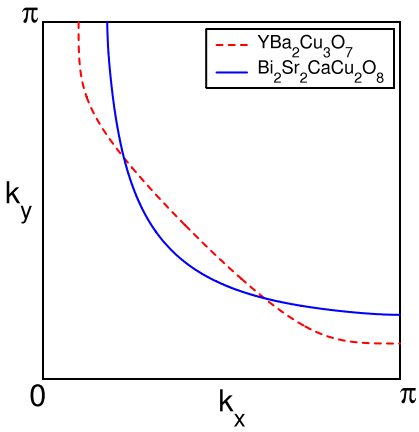

Figure 3. Fermi surfaces of $YBa_2Cu_3O_7$ (dashed) and $Bi_2Sr_2CaCu_2O_8$ (solid) adopted from fits to photoemission experiments [20, 21]. The corresponding model parameters are summarized in table 1.

Table 1. Tight-binding parameters for $YBa_2Cu_3O_7$ and $Bi_2Sr_2CaCu_2O_8$. The values for the hopping parameters are taken from [20] and [21]. The model-specific constant is $P_{\rm eff} \simeq 0.7$.

	Parameters (meV)					
	μ	$P_{\rm eff}t_1$	$P_{\rm eff}t_2$	$P_{\rm eff}t_3$	$P_{\rm eff}t_4$	$P_{\rm eff}t_5$
$YBa_2Cu_3O_7$	119	147	−36.5	−2.4	32.4	−1.8
$Bi_2Sr_2CaCu_2O_8$	49.4	73.9	−12.0	16.3	6.3	−11.7

$$\Delta_{\mathbf{k}}(T) = \frac{\Delta_0}{2}\left(\cos k_x - \cos k_y\right)\tanh\left(1.76\sqrt{T_{\rm c}/T - 1}\right), \tag{17}$$

where Δ_0 is considered to be a model parameter. We would like to point out that this formula is a fit to the solution of the Eliashberg strong-coupling gap equation.

In the forthcoming sections we will analyse several experiments in the superconducting state of the materials $YBa_2Cu_3O_7$ and $Bi_2Sr_2CaCu_2O_8$. We would like to summarize at this point the parameters which we used to perform our analysis. The tight-binding hopping parameters ($P_{\rm eff}t_1 \ldots P_{\rm eff}t_5$) are adopted from fits to the measured Fermi surfaces of these two materials, summarized in table 1. The corresponding Fermi surfaces are shown in figure 3. Note that they are quite different for these two materials.

Other model parameters include the gap parameter which is assumed to be of the order of $\Delta_0 \simeq 10$–30 meV and the superexchange interaction parameter of the copper spins, which is $J_1 \simeq 100$–140 meV. In our analysis we will proceed as follows. We assume the Fermi surface as given from fits to photoemission data and thus fix the values of the hopping parameters for both materials. Based on this assumption we analyse neutron scattering experiments, which allows us to determine the values of the model parameters Δ_0 and J_1. Then we move to NMR experiments and calculate the temperature dependences of the spin shift, spin–spin relaxation and spin–lattice relaxation rates, utilizing the parameter values obtained before. Thus in our analysis we fix our parameter values by analysing four different types of experiment. The fundamental difference between our description and the conventional RPA case [1–5] is that we do not need an effective interaction parameter $U_{\rm e}$ (sometimes this parameter is also called J); instead we use at least partially known experimental parameters, the gap and the superexchange parameter. In the RPA theory a fit to experiments is only possible if unusually large (even larger than the bandwidth) values for the effective interaction parameter are used. This means that the RPA description is not self-consistent. In our model, however, the spin susceptibility contains

two additional functions: $\Pi(\mathbf{q}, \omega)$ and $Z(\mathbf{q}, \omega)$. Together with the superexchange interaction parameter J_1 they provide a reasonable quantitative description of U_e.

3. Neutron scattering analysis

Magnetic inelastic neutron scattering experiments directly probe the imaginary part of the dynamical spin susceptibility $\mathrm{Im}\,\chi^{+,-}(\mathbf{q}, \omega)$. The experiments indicate a sharp resonance in the magnetic excitation spectrum of optimally doped $YBa_2Cu_3O_7$ [22, 23] and $Bi_2Sr_2CaCu_2O_8$ [24, 25] compounds at a frequency $\omega \simeq 41$ meV, near the antiferromagnetic wavevector $\mathbf{Q} = (\pi, \pi)$. Consequently, there should be a large peak in the imaginary part of the spin susceptibility $\mathrm{Im}\,\chi^{+,-}(\mathbf{Q}, \omega)$ at the same frequency. In the conventional weak-coupling scenario this feature was studied extensively by various authors [7–9], who connected the appearance of the resonance peak to a collective spin-density wave mode formation. Special experimental features like the effect of orthorhombic distortions [26] and bilayer splitting [27] on the magnetic excitations were also studied theoretically [9, 28] within the weak-coupling model. In the strong-coupling limit previous calculations were carried out by some of us [15] and the dependence of the position of the resonance peak on the model parameters was studied extensively. We will not repeat these considerations here. Note only that within our model the position of the neutron scattering resonance peak is determined mainly by the magnitude of the superconducting gap Δ_0 and the superexchange parameter J_1. In particular, the superconducting gap parameter Δ_0 determines the size of the transparency window in $\mathrm{Im}\,\chi^{+,-}(\mathbf{q}, \omega)$, which is approximately $\omega \simeq 2\Delta_0$. In this region a sharp delta-like peak appears in the imaginary part of the susceptibility if the resonance condition $1 + J_{\mathbf{q}}\,\mathrm{Re}\,\chi_0^{+,-}(\mathbf{q}, \omega) + \mathrm{Re}\,\Pi(\mathbf{q}, \omega) + \mathrm{Re}\,Z(\mathbf{q}, \omega) = 0$ (see (13)) is fulfilled. Our calculations indicate that for $YBa_2Cu_3O_7$ ($Bi_2Sr_2CaCu_2O_8$) the value of the gap parameter should be $\Delta_0 = 24$ meV (25 meV). The corresponding values of the superexchange parameter are determined as $J_1 = 90$ meV (110 meV). For these values the resonance condition is fulfilled and a clear peak appears in the imaginary part of the susceptibility near $\omega \simeq 41$ meV, for both materials. In figure 4 we display the calculated momentum and frequency dependence of the imaginary part of the susceptibility. Note that the height of the resonance peak depends on the artificially introduced quasiparticle damping Γ; therefore the values of $\mathrm{Im}\,\chi^{+,-}(\mathbf{q}, \omega)$ in figure 4 are arbitrary. Furthermore, the experimentally reported [29] downward dispersion branch for $YBa_2Cu_3O_7$ with respect to ω is reproduced by our model calculations, as can be seen from an inspection of figure 4 (top). We would like to point out that for the $Bi_2Sr_2CaCu_2O_8$ compound we do not find a similar dispersion branch. There are, however, no experiments available which would allow a comparison.

Let us now turn to the examination of magnetic excitations at lower frequency, where measurements [30] in the YBaCuO compounds indicate well defined incommensurability in the magnetic excitation spectrum. For the material $Bi_2Sr_2CaCu_2O_8$, however, the data sets [31] are inconclusive due to experimental difficulties. Here we report significant differences in the low-frequency excitations for the materials $YBa_2Cu_3O_7$ and $Bi_2Sr_2CaCu_2O_8$. Similar conclusions were reached previously by Norman [32] in the conventional weak-coupling scenario. In figure 5 we show an intensity plot of the imaginary part of the susceptibility around the antiferromagnetic wavevector $\mathbf{Q}$ calculated for $\omega = 30$ meV, for both materials. By examination of the figure we conclude that for $YBa_2Cu_3O_7$ the model calculations match the experimental observation [30] of incommensurability. For the $Bi_2Sr_2CaCu_2O_8$ compound, however, our results indicate that the incommensurability of the magnetic excitations is much weaker than in $YBa_2Cu_3O_7$ due to the difference in the Fermi surface topology. This result could be tested by further experiments.

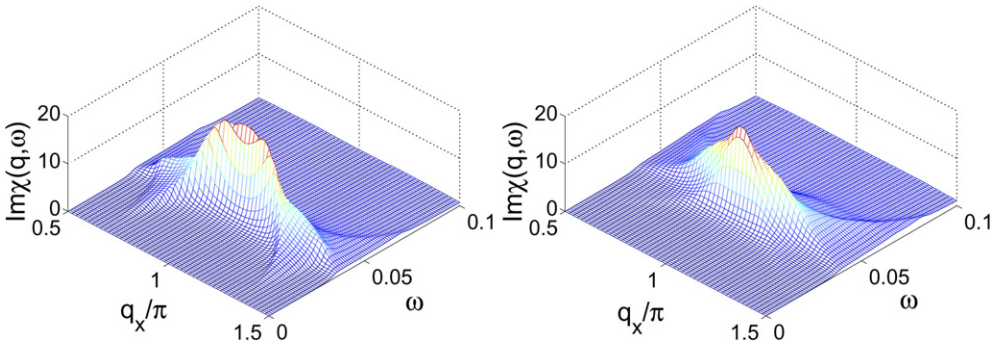

Figure 4. Calculated frequency and momentum dependence of $\mathrm{Im}\,\chi^{+,-}(\mathbf{q},\omega)$ for $YBa_2Cu_3O_7$ (left) and $Bi_2Sr_2CaCu_2O_8$ (right). The model parameters for the two compounds $YBa_2Cu_3O_7$ ($Bi_2Sr_2CaCu_2O_8$) are $\Delta_0 = 24$ meV (25 meV) and $J_1 = 90$ meV (110 meV). Furthermore, the tight-binding parameters are given in table 1.

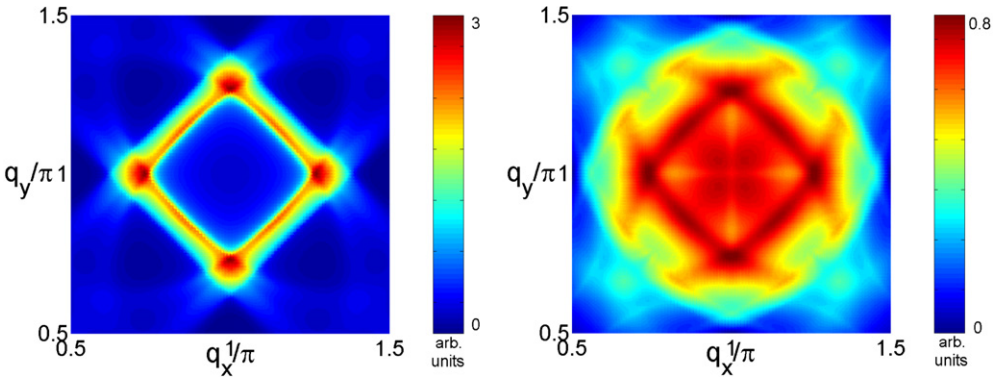

Figure 5. Intensity plot of the imaginary part of the susceptibility $\mathrm{Im}\,\chi^{+,-}(\mathbf{q},\omega)$ near $\mathbf{Q}$ for $YBa_2Cu_3O_7$ (left) and $Bi_2Sr_2CaCu_2O_8$ (right) for $\omega = 30$ meV. Other model parameters are the same as in figure 4.

4. NMR analysis

4.1. Knight shift

In order to calculate the Knight shift in the superconducting state we need to calculate the susceptibility in the limit $\mathbf{q} \to 0$, $\omega = 0$. The BCS susceptibility $\chi_0^{+,-}(\mathbf{q},\omega)$ converts to the Yosida result [33]

$$\chi_0^{+,-}(\mathbf{q} \to 0, \omega = 0) \simeq \frac{P\beta}{N} \sum_{\mathbf{k}} \frac{\partial f(E_{\mathbf{k}})}{\partial E_{\mathbf{k}}} = \chi_P. \tag{18}$$

The functions $\Pi(\mathbf{q},\omega)$ and $Z(\mathbf{q},\omega)$ are approximated as

$$\begin{aligned} \Pi(\mathbf{q} \to 0, \omega = 0) &\simeq \frac{1}{N} \sum_{\mathbf{k}} f(E_{\mathbf{k}}) - \frac{P\beta}{N} \sum_{\mathbf{k}} t_{\mathbf{k}} \frac{\partial f(E_{\mathbf{k}})}{\partial E_{\mathbf{k}}} \\ &\simeq \frac{\delta}{P} - \frac{P\beta}{N} \sum_{\mathbf{k}} t_{\mathbf{k}} \frac{\partial f(E_{\mathbf{k}})}{\partial E_{\mathbf{k}}} \end{aligned} \tag{19}$$

and

$$Z(\mathbf{q} \to 0, \omega = 0) \simeq P. \tag{20}$$

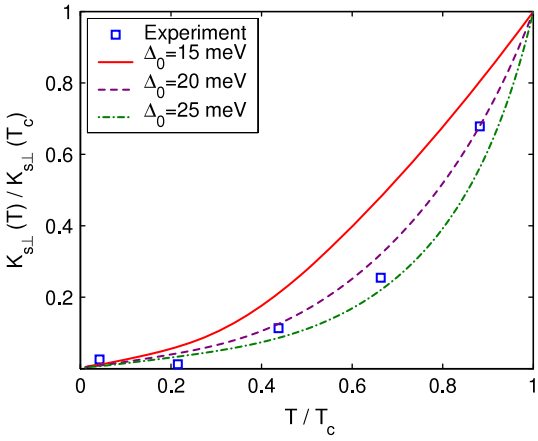

Figure 6. Temperature dependence of the reduced spin shift in $YBa_2Cu_3O_7$ for no exchange interaction ($J_1 = 0$ eV). The tight-binding parameters used are given in table 1. The experimental points are taken from Barrett *et al* [34].

In the long-wave limit therefore the susceptibility is given by the simple expression

$$\chi^{+,-}(\mathbf{q} \to 0, \omega = 0) = \frac{\chi_P}{1 + P + \delta/P + (2J_1 - \mu/P)\,\chi_P}. \tag{21}$$

With the help of this relation the spin shift can be calculated according to

$$^{63}K_{s\perp} = (A_\perp + 4B)\,\chi^{+,-}(\mathbf{q} \to 0, \omega = 0), \tag{22}$$

where $A_\perp$ and B represents the appropriate hyperfine coupling constants. Note that this expression refers to the spin contribution to the magnetic shift. In addition there is an orbital (chemical) shift which, however, is independent of the temperature. We will calculate the temperature dependence of the normalized spin shifts $K_{s\perp}(T)/K_{s\perp}(T_c)$. In this way the hyperfine coupling constants in (22) cancel out, simplifying our analysis. Furthermore, note that the quasiparticle damping is $\Gamma \to 0^+$.

It is also of interest, however, to determine the absolute values of the spin shift for comparison with experiments. For this reason we have calculated the values of the spin shift at $T = T_c = 90$ K. We must keep in mind that the absolute values of the spin shift scale with the values of hyperfine coupling constants, which are not directly accessible by experiments. For the values $B \simeq 0.4\ \mu$eV, $A_\perp \simeq 0.75B$ we get $K_{s\perp}(T = 90\text{ K}) = 0.24\%$. The difference from the experimentally reported [34] value $K_{s\perp}(T = 90\text{ K}) = (0.30 \pm 0.02)\%$ is explainable with a 20% uncertainty of the hyperfine fields. We would also like to point out that if we drop our correction function $Z(\mathbf{q}, \omega)$ we get $K_{s\perp}(T = 90\text{ K}) = 0.50\%$, which confirms the importance of this correction.

In figure 6 we display the calculated temperature dependence of the normalized spin shifts for $YBa_2Cu_3O_7$, along with the experimental points of Barrett *et al* [34], for vanishing superexchange interaction $J_1 = 0$ eV and different values of the gap parameter Δ_0. We observe that below T_c the spin shifts depend strongly on the magnitude of the gap parameter Δ_0. This behaviour has also been found for the RPA susceptibility [5, 6].

Next we consider how the spin shift depends on the superexchange interaction J_1. In figure 7 the calculated spin shifts for different values of the superexchange interaction parameter J_1 are shown. We see that the temperature dependence of the Knight shift does not significantly change by adjusting the parameter J_1. Also, contrary to the RPA scenario, the superexchange coupling J_1 reduces the rapid decrease of the Knight shift. By analysis of the figure we conclude that the optimal set of parameters to describe the experimentally observed temperature dependence of the spin shift for $YBa_2Cu_3O_7$ is $\Delta_0 = 24$ meV and $J_1 = 90$ meV

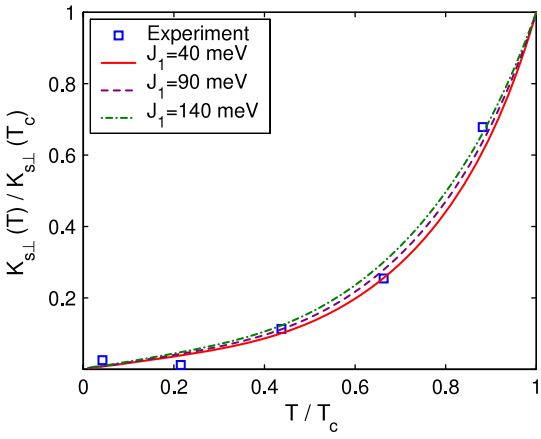

Figure 7. Temperature dependence of the reduced spin shift in $YBa_2Cu_3O_7$. The energy gap is $\Delta_0 = 24$ meV. The tight-binding parameters are given in table 1. The experimental points are taken from Barrett *et al* [34].

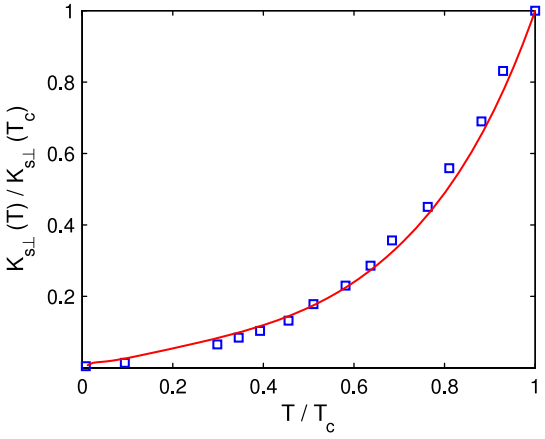

Figure 8. Temperature dependence of the reduced spin shift in $Bi_2Sr_2CaCu_2O_8$. The parameters used are $\Delta_0 = 24$ meV and $J_1 = 110$ meV. Furthermore, the tight-binding parameters are summarized in table 1. The experimental points are taken from Ishida *et al* [35].

for the given Fermi surface. These values are in perfect agreement with those determined from the fit to neutron scattering experiments in the previous section.

Let us now turn to the examination of the spin shift in the $Bi_2Sr_2CaCu_2O_8$ compound. Experimental results indicate a similar behaviour as in the $YBa_2Cu_3O_7$ material: the spin shift decreases rapidly upon entering the superconducting state. The calculated spin shifts also show a similar dependence on the model parameters Δ_0 and J_1. We will not repeat the analysis of these dependences and show instead in figure 8 the final result of our calculations for the spin shift in $Bi_2Sr_2CaCu_2O_8$ along with the experimental points of Ishida *et al* [35]. The parameters used for the calculation are $\Delta_0 = 24$ meV and $J_1 = 110$ meV. We notice that again these values almost coincide with those determined by the analysis of neutron scattering experiments in this compound. By examination of the figure we see that the calculated temperature dependence of spin shift gives a satisfactory fit to the experimental data.

Finally, we conclude that it is possible to account for both the neutron scattering resonance peak and the temperature dependence of the spin shift in the superconducting state of $YBa_2Cu_3O_7$ and $Bi_2Sr_2CaCu_2O_8$ consistently within the same set of parameters for each material. Next, we calculate the temperature dependence of the dynamical NMR quantities, the spin–spin and spin–lattice relaxation rates.

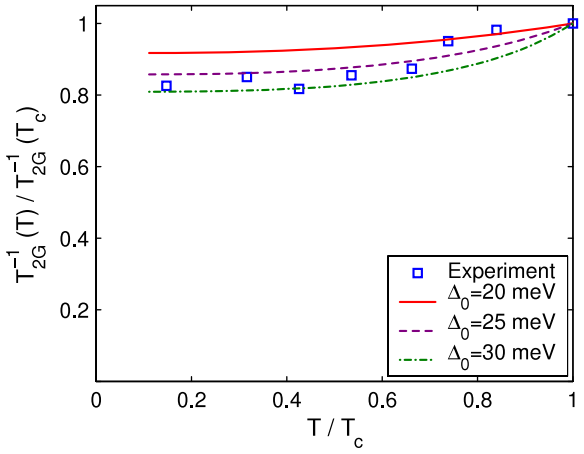

Figure 9. Temperature dependence of the spin–spin relaxation rate in $YBa_2Cu_3O_7$ for no exchange interaction ($J_1 = 0$ eV). Further parameters are given in table 1. The experimental points are taken from Stern *et al* [37].

4.2. Spin–spin relaxation

The nuclear spin–spin relaxation rate is calculated from the expression [36]

$$T_{2G}^{-2} = \frac{0.69}{m\hbar^2}\left[\frac{1}{N}\sum_{\mathbf{q}} {}^{63}F_{\parallel}(\mathbf{q})^2(\mathrm{Re}\,\chi^{+,-}(\mathbf{q},\omega=0))^2 - \left(\frac{1}{N}\sum_{\mathbf{q}} {}^{63}F_{\parallel}(\mathbf{q})\,\mathrm{Re}\,\chi^{+,-}(\mathbf{q},\omega=0)\right)^2\right], \tag{23}$$

where ${}^{63}F_{\parallel}(\mathbf{q}) = [A_{\parallel} + 2B(\cos(q_x) + \cos(q_y))]^2$ is the hyperfine form factor and m is a constant dependent on the method used ($m = 8$ for NMR and $m = 4$ for NQR measurements). The values of the hyperfine coupling constants are taken as $B \simeq 0.4$ μeV and $A_{\parallel} \simeq -4B$. The spin–spin relaxation rate strongly depends on the real part of the susceptibility $\mathrm{Re}\,\chi^{+,-}(\mathbf{q},\omega=0)$ near the antiferromagnetic wavevector $\mathbf{Q}$. We determine the temperature dependence of the normalized spin–spin relaxation rate $T_{2G}^{-1}(T)/T_{2G}^{-1}(T_c)$ in the same way as we analysed the Knight shifts. The absolute values of the spin–spin relaxation were calculated at $T = T_c = 90$ K. For the above-mentioned values of the hyperfine coupling constants we get $T_{2G}^{-1}(T = 90\ \mathrm{K}) = 7.4\ \mathrm{m\,s^{-1}}$. The difference from the experimental [37] value $T_{2G}^{-1}(T = 90\ \mathrm{K}) = 10\ \mathrm{m\,s^{-1}}$ could again be explained by a 20% uncertainty of the hyperfine fields. Note that for the evaluation of the spin–spin relaxation, the real part of the susceptibility is calculated by taking the quasiparticle damping $\Gamma \to 0^+$. Otherwise, due to the behaviour of the coherence factors, a large increase in the spin–spin relaxation rate occurs near T_c upon entering the superconducting state, as has been discussed in [36].

In figure 9 we display the calculated spin–spin relaxation rates for $YBa_2Cu_3O_7$ along with experimental points from Stern *et al* [37] for no superexchange interaction $J_1 = 0$ eV. We observe that the results show a similar temperature dependence as in the RPA approach [6]. Generally, the temperature dependence of the spin–spin relaxation rate is less sensitive to the change of the gap parameter than the spin shift. We see that for the hypothetical case of no interaction we can account for the observed temperature dependence of the spin–spin relaxation rate. Next we wish to study the behaviour of the spin–spin relaxation for different values of the superexchange interaction parameter J_1.

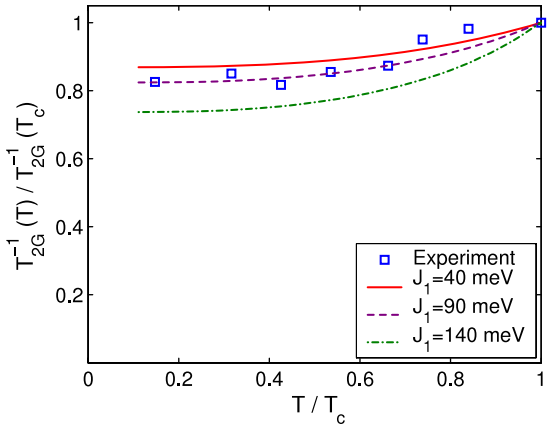

Figure 10. Temperature dependence of the spin–spin relaxation rate in $YBa_2Cu_3O_7$. The energy gap is $\Delta_0 = 22$ meV. The corresponding tight-binding parameters are summarized in table 1. The experimental points are taken from Stern *et al* [37].

In figure 10 the temperature dependence of the spin–spin relaxation rate is shown for various values of the superexchange interaction parameter J_1. We see that we get a reasonable agreement with the data using the parameter values $\Delta_0 = 22$ meV and $J_1 = 90$ meV. The magnitudes of these parameters are in agreement with those obtained by the analysis of neutron scattering and NMR spin shift experiments for $YBa_2Cu_3O_7$.

Concerning the $Bi_2Sr_2CaCu_2O_8$ compound our calculations indicate a very similar behaviour as in $YBa_2Cu_3O_7$, if we utilize the parameter values from the previous sections $\Delta_0 = 24$ meV and $J_1 = 110$ meV. Unfortunately the spin–spin relaxation rate has not yet been measured in $Bi_2Sr_2CaCu_2O_8$, thus we have no basis for comparison with experiments.

4.3. Spin–lattice relaxation

The nuclear spin–lattice relaxation rate is calculated according to the expression [38]

$$ {}^{\alpha}T_{1\beta}^{-1} \propto \frac{T}{N} \sum_{\mathbf{q},\beta'} {}^{\alpha}F_{\beta'}(\mathbf{q}) \lim_{\omega\to 0} \frac{\operatorname{Im}\chi^{+,-}(\mathbf{q},\omega)}{\omega}, \tag{24} $$

where β denotes the field direction and β' are the directions orthogonal to the field. Furthermore, α designates the nucleus under consideration.

In order to calculate the imaginary part of the spin susceptibility $\operatorname{Im}\chi^{+,-}(\mathbf{q},\omega\to 0)$ we introduced a finite quasiparticle broadening $\Gamma = 3k_BT_c \simeq 2$ meV, following the analysis of Bulut and Scalapino [5]. Furthermore, the form factors in (24) are given by

$$ \begin{aligned} {}^{63}F_{\beta}(\mathbf{q}) &= \left[A_\beta + 2B\left(\cos(q_x)+\cos(q_y)\right)\right]^2, \\ {}^{17}F_{\beta}(\mathbf{q}) &= 2\left(C_{\beta_1}^2\cos^2(q_x/2) + C_{\beta_2}^2\cos^2(q_y/2)\right). \end{aligned} \tag{25} $$

The values of the hyperfine coupling constants are taken as $B \simeq 0.4$ μeV, $A_\parallel \simeq -4B$, $A_\perp \simeq 0.75B$, $C_\parallel \simeq 0.6B$, and $C_\perp \simeq 0.32B$.

In figure 11 we display the calculated spin–lattice relaxation rates for $YBa_2Cu_3O_7$ along with the experimental points of Takigawa *et al* [39], when the superexchange interaction is $J_1 = 0$ eV. We observe that the temperature dependence varies strongly when adjusting the gap parameter Δ_0. As for the spin shift and spin–spin relaxation rate calculations it is possible to fit the experimental data even without taking into account the interaction.

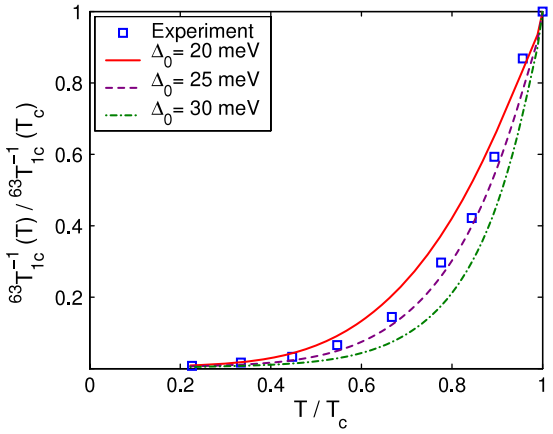

Figure 11. Temperature dependence of the spin–lattice relaxation rate in $YBa_2Cu_3O_7$ for no exchange interaction ($J_1 = 0$ eV). Corresponding tight-binding parameters are given in table 1. The experimental points are taken from Takigawa *et al* [39].

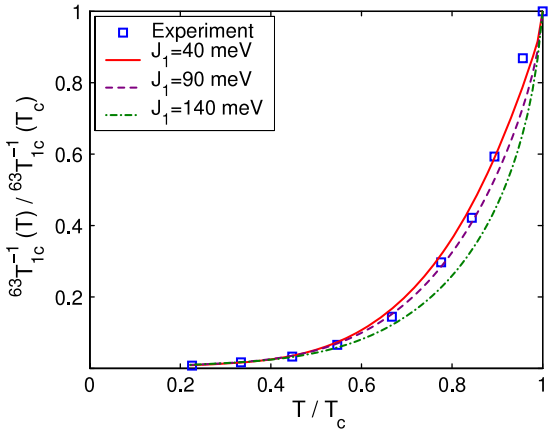

Figure 12. Temperature dependence of the spin–lattice relaxation rate in $YBa_2Cu_3O_7$. The energy gap is $\Delta_0 = 22$ meV. The tight-binding parameters are given in table 1. The experimental points are taken from Takigawa *et al* [39].

Next we consider the effect of the superexchange parameter J_1. In figure 12 the spin–lattice relaxation rate is shown for different values of J_1. We note that upon changing the values of J_1 the spin–lattice relaxation rate T_{1c}^{-1} changes in the same way as it does in the RPA case if the parameter value of the effective Coulomb interaction U_e is changed. Namely, the parameter J_1 has no significant impact on the temperature dependence of the spin–lattice relaxation rate in the superconducting state. Upon further examination of the figure we see that we get a reasonable agreement with experimental observation using the parameter values $\Delta_0 = 22$ meV and $J_1 = 90$ meV. These parameters agree with those we determined before in the previous sections.

Next we examine the spin–lattice relaxation rate in the $Bi_2Sr_2CaCu_2O_8$ compound. Upon changing the model parameters Δ_0 and J_1 the spin–lattice relaxation behaves much the same way as in $YBa_2Cu_3O_7$. We show in figure 13 the final result of our calculations of the spin–lattice relaxation rate in $Bi_2Sr_2CaCu_2O_8$, along with the experimental points of Ishida *et al* [35] (squares) and Takigawa *et al* [40] (circles). The parameters used for the calculation are

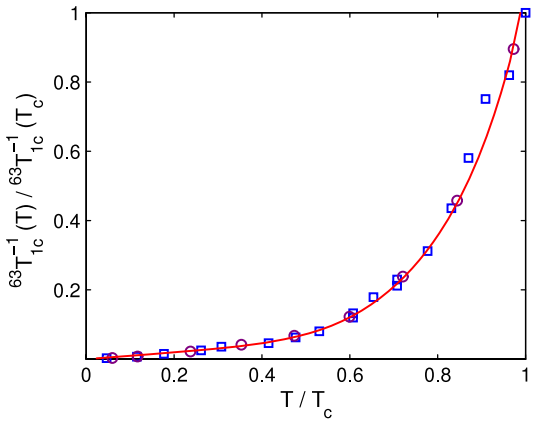

Figure 13. Temperature dependence of the spin–lattice relaxation rate in $Bi_2Sr_2CaCu_2O_8$. The parameters are $\Delta_0 = 23$ meV and $J_1 = 110$ meV. Furthermore, the tight-binding parameters are given in table 1. The experimental points are taken from Ishida *et al* [35] (squares) and Takigawa *et al* [40] (circles).

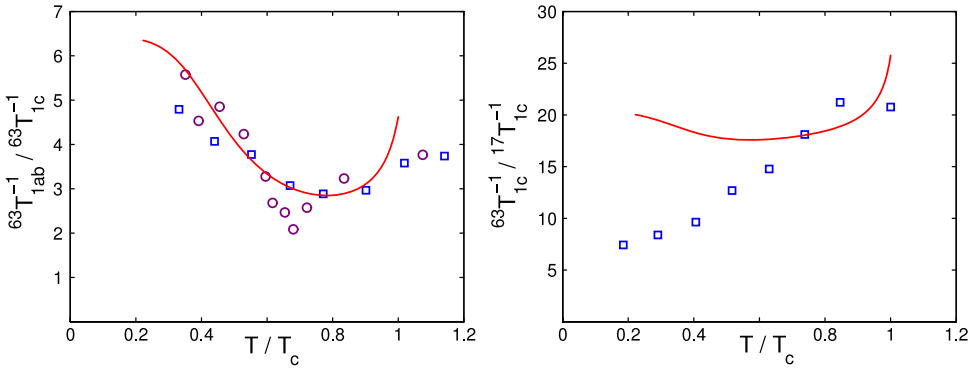

Figure 14. Calculated temperature dependence of the anisotropy ratios $^{63}T_{1c}^{-1}/^{17}T_{1c}^{-1}$ and $^{63}T_{1ab}^{-1}/^{63}T_{1c}^{-1}$ in $YBa_2Cu_3O_7$ (solid lines). The data from [42] are denoted by squares. For comparison we also included data from [43] for $YBa_2Cu_4O_8$ (circles). The model parameters are $\Delta_0 = 22$ meV and $J_1 = 90$ meV.

$\Delta_0 = 23$ meV and $J_1 = 110$ meV. Note that the values of these parameters are again almost the same as those that we used before when we analysed the neutron scattering and spin shift experiments. A particularly interesting feature can be found when comparing the spin–lattice relaxation rates in $YBa_2Cu_3O_7$ and $Bi_2Sr_2CaCu_2O_8$ at low temperatures. A close inspection of the corresponding figures (figures 12 and 13) shows that in the former case $^{63}T_{1c}^{-1}(T)$ practically vanishes at temperatures $T < 20$ K, while in the latter case the relaxation rate seems to vanish only at $T \simeq 0$ K. Note that both of these dependences are reproduced by the model calculations.

We are also interested in the anisotropy ratios $^{63}T_{1ab}^{-1}/^{63}T_{1c}^{-1}$ and $^{63}T_{1c}^{-1}/^{17}T_{1c}^{-1}$ measured in $YBa_2Cu_3O_7$. Experimental evidence [41–43] points towards a field dependence of these quantities. Our theoretical results have to be compared with data in zero or small external fields. We display the calculated anisotropy ratios in figure 14. The experimental points for $^{63}T_{1c}^{-1}/^{17}T_{1c}^{-1}$ are from Martindale *et al* [41], whereas those for $^{63}T_{1ab}^{-1}/^{63}T_{1c}^{-1}$ are taken from Takigawa *et al* [42] (squares). For comparison we also plotted the anisotropy in the $YBa_2Cu_4O_8$ compound (circles) measured by Bankay *et al* [43]. For the calculation we

used the same parameters as before, $\Delta_0 = 22$ meV and $J_1 = 90$ meV. We see that we can account for the anisotropy ratio ${}^{63}T_{1ab}^{-1}/{}^{63}T_{1c}^{-1}$, but it is not possible to reproduce the temperature dependence of the ratio ${}^{63}T_{1c}^{-1}/{}^{17}T_{1c}^{-1}$. Our results for the weak-field anisotropy ratio ${}^{63}T_{1ab}^{-1}/{}^{63}T_{1c}^{-1}$ for $YBa_2Cu_3O_7$ agree with the weak-coupling calculations of Bulut and Scalapino [5], which are based on a square Fermi surface with nearest-neighbour hopping only. However, our calculations disagree with the analysis of Mack *et al* [6], where the Fermi surface for $YBa_2Cu_3O_7$ was assumed to be quite different (similar to that which we used here to describe the $Bi_2Sr_2CaCu_2O_8$ compound). Therefore we conclude that the Fermi surface topology plays an important role in the description of the weak-field anisotropy ratio ${}^{63}T_{1ab}^{-1}/{}^{63}T_{1c}^{-1}$. Note that the experimentally reported weak-field ratio ${}^{63}T_{1c}^{-1}/{}^{17}T_{1c}^{-1}$ could also not be reproduced within previous weak-coupling RPA calculations [5, 6].

5. Conclusions

In summary, we have determined the spin susceptibility in cuprates within a special Hubbard model which includes strong correlation effects. It has been found that the susceptibility in the strong-coupling limit is different from the standard Pauli–Lindhard formula. In particular, two correction functions were determined in the superconducting state. The first one, $\Pi(\mathbf{q}, \omega)$, found originally by Hubbard and Jain [14] in the normal state, originates from the anticommutator rule which is modified due to the Coulomb repulsion, whereas the function $Z(\mathbf{q}, \omega)$ has its origin in the fast fluctuations of the localized spins and was previously discussed by Zavidonov and Brinkmann [12] for the normal state.

We analysed inelastic neutron scattering and NMR data in the superconducting state of the optimally doped high-T_c superconductors $YBa_2Cu_3O_7$ and $Bi_2Sr_2CaCu_2O_8$. In our analysis we have taken into account the experimentally measured topology of the Fermi surface, which is quite different for these two materials. We found that on the whole the results within the strong-coupling and weak-coupling limits agree with each other. Based on the results of our numerical calculations we conclude that strong correlation effects, i.e., the effect of the functions $\Pi(\mathbf{q}, \omega)$, $Z(\mathbf{q}, \omega)$ on the susceptibility can be modelled in the weak-coupling approach by an appropriate redefinition [28] of the effective Coulomb interaction parameter U_e. In particular, the non-physical value of U_e in the weak-coupling limit (sometimes $U_e \geqslant t$) becomes understandable. In terms of our model, it can be explained quantitatively by the superexchange interaction $J_{\mathbf{q}}$ and the two additional functional corrections $\Pi(\mathbf{q}, \omega)$ and $Z(\mathbf{q}, \omega)$.

In the framework of the singlet-correlated band model we found it possible to describe the available experimental data in the optimally doped $YBa_2Cu_3O_7$ and $Bi_2Sr_2CaCu_2O_8$ compounds within one set of model parameters for each material. These optimal sets of parameters are given by $\Delta_0 = 23$ meV ($\pm 5\%$), $J_1 = 90$ meV for $YBa_2Cu_3O_7$ and $\Delta_0 = 24$ meV ($\pm 5\%$), $J_1 = 110$ meV for $Bi_2Sr_2CaCu_2O_8$. The only experiment which could not be reproduced is the temperature dependence of the weak-field anisotropy ratio ${}^{63}T_{1c}^{-1}/{}^{17}T_{1c}^{-1}$ in $YBa_2Cu_3O_7$. As concerns the $Bi_2Sr_2CaCu_2O_8$ material, more experimental data would be desirable to test our model further, for example low-energy inelastic neutron scattering and spin–spin relaxation rate measurements.

Acknowledgments

This work is supported by the Swiss National Science Foundation. M Eremin is partially supported by the Russian Grant (RFBR No 06-02-17197-a) and SCOPES program (Grant No IB7420-110784). We would like to thank M Mali and J Roos for fruitful discussions.

References

[1] Bulut N, Hone D W, Scalapino D J and Bickers N E 1990 *Phys. Rev.* B **41** 1797
[2] Bulut N, Hone D, Scalapino D J and Bickers N E 1990 *Phys. Rev. Lett.* **64** 2723
[3] Bulut N and Scalapino D J 1991 *Phys. Rev. Lett.* **67** 2898
[4] Bulut N and Scalapino D J 1992 *Phys. Rev. Lett.* **68** 706
[5] Bulut N and Scalapino D J 1992 *Phys. Rev.* B **45** 2371
[6] Mack F, Kulic M L and Mehring M 1998 *Physica* C **295** 136
[7] Onufrieva F and Rossat-Mignod J 1995 *Phys. Rev.* B **52** 7572
[8] Onufrieva F and Pfeuty P 2002 *Phys. Rev.* B **65** 054515
[9] Brinckmann J and Lee P A 2001 *Phys. Rev.* B **65** 014502
[10] Weng Z Y, Sheng D N and Ting C S 1995 *Phys. Rev.* B **52** 637
[11] Sherman A and Schreiber M 2003 *Phys. Rev.* B **68** 094519
Sega I, Prelovsek P and Bonca J 2003 *Phys. Rev.* B **68** 054524
[12] Zavidonov A Yu and Brinkmann D 1998 *Phys. Rev.* B **58** 12486
[13] Eremin M, Eremin I and Varlamov S 2001 *Phys. Rev.* B **64** 214512
[14] Hubbard J and Jain K P 1968 *J. Phys. C: Solid State Phys.* **1** 1650
[15] Eremin I, Kamaev O and Eremin M V 2004 *Phys. Rev.* B **69** 094517
[16] Zhang F C and Rice T M 1988 *Phys. Rev.* B **37** R3759
[17] Nucker N, Fink J, Fuggle J C, Durham P J and Temmerman W M 1988 *Phys. Rev.* B **37** 5158
[18] Eremin M, Solov'yanov S G and Varlamov S V 1997 *JETP* **85** 963
[19] Mayer T 2005 http://www.dissertationen.unizh.ch/2005/mayer/diss.pdf
[20] Norman M R 2000 *Phys. Rev.* B **63** 092509
[21] Eschrig M and Norman M R 2003 *Phys. Rev.* B **67** 144503
[22] Bourges P, Regnault L P, Sidis Y and Vettier C 1996 *Phys. Rev.* B **53** 876
[23] Mook H A, Yethiraj M, Aeppli G, Mason T E and Armstrong T 1993 *Phys. Rev. Lett.* **70** 3490
[24] Fong H, Bourges P, Sidis Y, Regnault L P, Ivanov A, Gu G D, Koshizuka N and Keimer B 1999 *Nature* **398** 588
[25] He H, Sidis Y, Bourges P, Gu G D, Ivanov A, Koshizuka N, Liang B, Lin C T, Regnault L P, Schoenherr E and Keimer B 2001 *Phys. Rev. Lett.* **86** 1610
[26] Hinkov V, Pailhes S, Bourges P, Sidis Y, Ivanov A, Kulakov A, Lin C T, Chen D P, Bernhard C and Keimer B 2004 *Nature* **430** 650–4
[27] Pailhes S *et al* 2003 *Phys. Rev. Lett.* **91** 237002
[28] Eremin I and Manske D 2005 *Phys. Rev. Lett.* **94** 067006
[29] Reznik D, Bourges P, Pintschovius L, Endoh Y, Sidis Y, Masui T and Tajima S 2004 *Phys. Rev. Lett.* **93** 207003
[30] Mook H A, Dai P, Hayden S M, Aeppli G, Perring T G and Dogan F 1998 *Nature* **395** 580
[31] Mook H A, Dogan F and Chakoumakos B C 1998 *Preprint* cond-mat/9811100
[32] Norman M R 2000 *Phys. Rev.* B **61** 14751
[33] Yosida K 1958 *Phys. Rev.* **110** 769
[34] Barrett S E, Durand D J, Pennington C H, Slichter C P, Firedmann T A, Rice J P and Ginsberg D M 1990 *Phys. Rev.* B **41** 6283
[35] Ishida K, Yoshida K, Mito T, Tokunaga Y, Kitaoka Y and Asayama K 1998 *Phys. Rev.* B **58** R5960
[36] Thelen D and Pines D 1994 *Phys. Rev.* B **49** 3528
[37] Stern R, Mali M, Roos J and Brinkmann D 1995 *Phys. Rev.* B **51** 15478
[38] Moriya T 1963 *J. Phys. Soc. Japan* **18** 516–23
[39] Takigawa M, Reyes A P, Hammel P C, Thompson J D, Heffner R H, Fisk Z and Ott K C 1991 *Phys. Rev.* B **43** 247
[40] Takigawa M and Mitzi D B 1994 *Phys. Rev. Lett.* **73** 1287
[41] Martindale J A, Barrett S E, O'Hara K E, Slichter C P, Lee W C and Ginsberg D M 1993 *Phys. Rev.* B **47** R9155
[42] Takigawa M, Smith J L and Huts W L 1991 *Phys. Rev.* B **44** R7764
[43] Bankay M, Mali M, Roos J, Mangelschots I and Brinkmann D 1992 *Phys. Rev.* B **46** R11228